Available online at www.sciencedirect.com

ScienceDirect

www.elsevier.com/locate/jes

JES JOURNAL OF ENVIRONMENTAL SCIENCES

www.jesc.ac.cn

Dosing low-level ferrous iron in coagulation enhances the removal of micropollutants, chlorite and chlorate during advanced water treatment

Gabriela Scheibel Cassol[1], *Chii Shang*[1], *Juan Li*[1,*], *Li Ling*[1], *Xin Yang*[2], *Ran Yin*[1,*]

[1] *Department of Civil and Environmental Engineering, The Hong Kong University of Science and Technology, Hong Kong 999066, China*

[2] *School of Environmental Science and Engineering, Guangdong Provincial Key Laboratory of Environmental Pollution Control and Remediation Technology, Sun Yat-sen University, Guangzhou 510275, China*

ARTICLE INFO

Article history:
Received 28 December 2021
Revised 24 February 2022
Accepted 14 March 2022
Available online 25 March 2022

Keywords:
Chlorine dioxide (ClO_2)
Advanced oxidation process
Ferrous iron
Micropollutants
Disinfection byproducts (DBPs)

ABSTRACT

Drinking water utilities are interested in upgrading their treatment facilities to enhance micropollutant removal and byproduct control. Pre-oxidation by chlorine dioxide (ClO_2) followed by coagulation-flocculation-sedimentation and advanced oxidation processes (AOPs) is one of the promising solutions. However, the chlorite (ClO_2^-) formed from the ClO_2 pre-oxidation stage cannot be removed by the conventional coagulation process using aluminum sulfate. ClO_2^- negatively affects the post-UV/chlorine process due to its strong radical scavenging effect, and it also enhances the formation of chlorate (ClO_3^-). In this study, dosing micromolar-level ferrous iron (Fe(II)) into aluminum-based coagulants was proposed to eliminate the ClO_2^- generated from ClO_2 pre-oxidation and benefit the post-UV/chlorine process in radical production and ClO_3^- reduction. Results showed that the addition of 52.1-μmol/L $FeSO_4$ effectively eliminated the ClO_2^- generated from the pre-oxidation using 1.0 mg/L (14.8 μmol/L) of ClO_2. Reduction of ClO_2^- increased the degradation rate constant of a model micropollutant (carbamazepine) by 55.0% in the post-UV/chlorine process. The enhanced degradation was verified to be attributed to the increased steady-state concentrations of $HO^{\cdot}$ and $ClO^{\cdot}$ by Fe(II) addition. Moreover, Fe(II) addition also decreased the ClO_3^- formation by 53.8% in the UV/chlorine process and its impact on the formation of chloro-organic byproducts was rather minor. The findings demonstrated a promising strategy to improve the drinking water quality and safety by adding low-level Fe(II) in coagulation in an advanced drinking water treatment train.

* Corresponding authors.
E-mails: lj_hit1@163.com (J. Li), ryin@connect.ust.hk (R. Yin).

https://doi.org/10.1016/j.jes.2022.03.022
1001-0742/© 2022 The Research Center for Eco-Environmental Sciences, Chinese Academy of Sciences. Published by Elsevier B.V.

Introduction

Drinking water utilities are working towards upgrading their treatment facilities to enhance micropollutant removal and byproduct control. Advanced oxidation processes (AOPs) are considered to be implemented after the conventional treatment units (referred to CTUs, including coagulation, flocculation, and sedimentation) to remove the emerging contaminants (Aghdam et al., 2017; Qin et al., 2014; Sichel et al., 2011; Wang et al., 2016; Xiang et al., 2016). However, the formation of undesired DBPs in these AOPs remains a concern (Liu et al., 2012; Ruan et al., 2021). Pre-oxidation prior to CTUs can reduce the formation of DBPs in the post-chlorination or AOP processes (Hu et al., 2018; Pai et al., 2020). For example, pre-oxidation by chlorine dioxide (ClO_2) is an effective way to reduce the formation of chloro-organic byproducts in the post-UV/chlorine process, because it can modify the natural organic matter (NOM) and makes it less reactive towards byproduct formation (Fan et al., 2022; Rougé et al., 2020). However, ClO_2 pre-oxidation generates chlorite (ClO_2^-), which negatively affects the post-UV/chlorine process even at low levels, because ClO_2^- is a strong radical scavenger (Zhao et al., 2021). Moreover, ClO_2^- as well as its oxidation product chlorate (ClO_3^-) are regulated disinfection byproducts (DBPs) in drinking water (Kim et al., 2017; Rougé et al., 2018). One strategy to improving the "ClO_2-CTUs-UV/chlorine process" is to eliminate the ClO_2^- during CTUs before it enters the UV/chlorine process.

Aluminum sulfate ($Al_2(SO_4)_3$) is the most commonly used coagulant in CTUs but it cannot reduce ClO_2^-. Herein, we propose to add small amounts (micromolar level) of ferrous iron (Fe(II)) to mix with $Al_2(SO_4)_3$ and to eliminate the low-level ClO_2^- formed from ClO_2 pre-oxidation. Fe(II) can effectively reduce ClO_2^- to Cl^- within a wide pH range of 5.0–10.0, following Eq. (1) (Henderson et al., 2001; Hurst and Knocke, 1997; Iatrou and Knocke, 1992; Yang et al., 2021). Meanwhile, Fe(II) is oxidized by ClO_2^- to ferric iron (Fe(III)) (Eq. (1)). The formed Fe(III) mainly exists in the form of insoluble ferric hydroxide ($Fe(OH)_3$) in water at pH > 3 (Behin et al., 2017), which could serve as a coagulant to remove NOM and suspended solids (Wang et al., 2020).

$$4Fe^{2+} + ClO_2^- + 10H_2O \rightleftharpoons 4Fe(OH)_{3(s)} + 4e^- + Cl^- + 8H^+ \quad (1)$$

Although ClO_2^- can be eliminated by other chemical reduction and/or adsorption approaches, these technologies suffer from some limitations. Adsorption requires the implementation of treatment units containing adsorbents (e.g., activated carbon) and the replacement or regeneration of the used adsorbents (Dixon and Lee, 1991; Hurst and Knocke, 1997). Chemical reduction using sulfite (SO_3^{2-}) can also reduce ClO_2^- to chloride (Cl^-), but it is only effective within a narrow pH range of 5.0–6.5 (Henderson et al., 2001). Comparatively, dosing low-level of Fe(II) with the $Al_2(SO_4)_3$ as the mixed coagulants is a cost-effective and easy-operating way to tackle the ClO_2^- issue. The added Fe(II) is expected to decrease the ClO_2^- concentration and reduce the radical scavenging effect of ClO_2^- in the UV/chlorine process. Consequently, the radical concentrations in the UV/chlorine process are hypothesized to increase compared to the scenario without Fe(II) addition, and the micropollutant degradation can be improved correspondingly. In addition, the formation of ClO_2^- and ClO_3^- in the entire treatment train is hypothesized to be reduced due to the reduction of ClO_2^- before it enters the UV/chlorine process. The formation of chloro-organic byproducts might also be affected due to the increase of radical concentrations in the UV/chlorine process.

This study was designed to verify the above hypotheses by investigating the effect of adding small amounts of Fe(II) during coagulation process on the (1) micropollutant degradation, (2) radical concentrations, (3) ClO_2^- and ClO_3^- formation, and (4) chloro-organic byproduct formation in the CTUs and the UV/chlorine process. Carbamazepine (CBZ) was selected as a representative micropollutant because (1) it has relatively high occurrence in surface water compared to other micropollutants (Benotti et al., 2009; Daughton, 2004; Pan et al., 2017), (2) and it cannot be effectively removed by CTUs (Pan et al., 2017) nor by chlorine/ClO_2 oxidation (Gan et al., 2020; Lee and von Gunten, 2010). The degradation of CBZ in the proposed treatment train (Fig. 1) with or without Fe(II) addition was investigated and compared. The radical concentrations in the post-UV/chlorine process with or without Fe(II) addition were quantified and compared. The concentrations of ClO_2^-, ClO_3^-, and chloro-organic byproducts formed in the proposed treatment train (Fig. 1) with or without Fe(II) addition were also determined and compared.

1. Materials and Methods

1.1. Chemicals

Sodium hypochlorite (NaOCl), sodium hydrogen phosphate (Na_2HPO_4), sodium dihydrogen phosphate (NaH_2PO_4), nitrobenzene (NB), benzoic acid (BA), 1,4-dimethoxybenzene (DMOB), N,N-diethyl-p-phenylenediamine (DPD), aluminum sulfate octadecahydrate ($Al_2(SO_4)_3{\cdot}18H_2O$), iron(II) sulfate heptahydrate ($FeSO_4{\cdot}7H_2O$), caffeine (CAF), ibuprofen (IBP), CBZ, ethylenediamine (EDA), sodium bicarbonate ($NaHCO_3$), potassium nitrate (KNO_3), calcium sulfate ($CaSO_4$), 5,5-Dimethyl-1-pyrroline N-oxide (DMPO), and ascorbic acid of reagent grades were purchased from Sigma-Aldrich. Phosphoric acid, methanol, and methyl tert-butyl ether (MTBE) of high-performance liquid chromatography (HPLC) grades were purchased from Fisher Scientific. The Suwannee River natural organic matter (SRNOM) isolates were purchased from the International Humic Substance Society (IHSS). The stock solutions were prepared by dissolving the chemicals in the deionized water (18.2 MΩ·cm) produced by a water purification system (Millipore, USA). Solutions were stored at 4°C in the dark and allowed to return to ambient temperature (22±2°C) before use. Standard solutions of chloro-organic byproducts including trihalomethanes (THMs), haloketones (HKs), haloacetonitriles (HANs), chloral hydrate (CH), and trichloronitromethane (TCNM) were purchased from Sigma-Aldrich. The ClO_2 stock solution was produced by acidifying $NaClO_2$ using H_2SO_4, following the Standard Methods (APHA, 2017). A free chlorine stock solution (about 1000 mg/L as Cl_2) was diluted from the 4%–5% NaOCl solution.

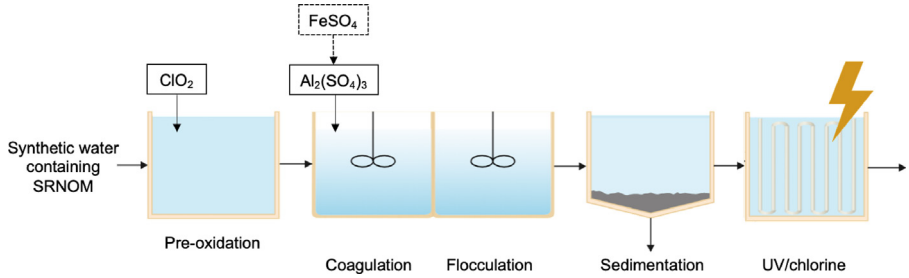

Fig. 1 – Schematic diagram of the drinking water treatment train proposed in this work.

1.2. *Experimental procedures*

1.2.1. *ClO_2 pre-oxidation*

All experiments were conducted at room temperature. Synthetic surface water containing SRNOM (3.0 mg/L as C), bicarbonate ion (30 mg/L as $NaHCO_3$), nitrate ion (1 mg/L as KNO_3), and calcium ion (30 mg/L as $CaSO_4$) was prepared in 2 mmol/L phosphate buffer at pH 6.5 (Zeng et al., 2019). Pre-oxidation was initiated by adding ClO_2 stock solution into a beaker containing 500 mL of the synthetic surface water (to give an initral ClO_2 concentration at 1.0 mg/L (14.8 µmol/L)) with a gentle mixing (40 r/min) provided by an overhead stirrer. Parallel samples were withdrawn after 30 min, filtered with a 0.22-µm membrane filter, and quenched with freshly prepared EDA followed by nitrogen gas purging for analysis of ClO_2^- and ClO_3^- (Gan et al., 2019), or quenched with freshly prepared ascorbic acid for analysis of residual concentrations of CBZ.

1.2.2. *Conventional treatment units (CTUs)*

Immediately after pre-oxidation with ClO_2, the 500 mL of water was treated by $Al_2(SO_4)_3$ (0.36 mmol/L as Al) with or without addition of $FeSO_4$ (52.1 µmol/L as Fe(II)). The Fe(II) dosage was chosen to be 1.2 times the stoichiometric requirement for ClO_2^- reduction to Cl^- (Eq. (1)), to ensure the fully elimination of ClO_2^- (Hurst and Knocke, 1997). After adding the coagulant, the solutions were rapidly mixed for 1 min at 200 r/min using an overhead stirrer, followed by a slow mixing at 40 r/min for 15 min and settling for another 30 min. After settling, the supernatant was collected, filtered with a 0.22-µm membrane filter, quenched with EDA followed by nitrogen gas purging, and subjected to the analysis of ClO_2^- and ClO_3^- concentrations (Gan et al., 2019), or quenched with ascorbic acid for the analysis of residual concentrations of CBZ. Another 200 mL of the supernatant was collected and transferred immediately to a UV reactor (Appendix A Fig. S1) for the subsequent treatment by the UV/chlorine process.

1.2.3. *UV/chlorine process*

Photochemical experiments were conducted using a bench-scale UV irradiator consisting of four low-pressure UV lamps (254 nm, G15T8, 10 W, Sankyo Denki) placed in a shuttered box, with a vertical collimating tube extending from the bottom (Appendix A Fig. S1). The glass batch reactor containing 200 mL of the sample was placed under the collimating tube and covered by a quartz sheet. The average UV intensity in the reactor was 0.33 mW/cm^2, which was determined using the iodide-iodate (KI/KIO_3) chemical actinometry (Bolton and Linden, 2003). NaOCl stock solution was added into the water sample to give an initial chlorine concentration of 70 µmol/L (5.0 mg/L) before UV irradiation. After chlorine addition, the mixed solution was immediately placed under the UV irradiation to initiate the UV/chlorine process. Samples were taken at predetermined time intervals, filtered with a 0.22-µm membrane filter, quenched with EDA, and subjected to the analysis of ClO_2^- and ClO_3^- concentrations (Gan et al., 2019), or quenched with ascorbic acid for analysis of residual concentrations of CBZ.

To determine the concentrations of radicals generated in the UV/chlorine process, experiments were conducted in the similar manner, expcept that NB, BA, and DMOB at 2.0 µmol/L each were added as probe compounds (Yin et al., 2019). The samples were collected at different time intervals during the UV/chlorine process (0–50 min), filtered by a 0.22-µm membrane, quenched with ascorbic acid, and subjected to the analysis of residual concentrations of the probe compounds.

1.3. *Analytical methods*

The concentration of ClO_2 stock solution was standardized by direct UV measurement at 359 nm ($\varepsilon_{359} = 1230$ (mol/L)$^{-1}$ cm^{-1}) (Furman and Margerum, 1998). The free chlorine stock solution was standardized by DPD/FAS titration (APHA, 2017). Free chlorine and ClO_2 residuals were determined using the DPD Colorimetric Method (4500-Cl G) (APHA, 2017). The concentrations of CBZ, CAF, IBP, NB, BA, and DMOB were determined using a high-performance liquid chromatograph (HPLC) (1260 Infinity II, Agilent) equipped with a Waters symmetry C18 column and a UV–Vis detector. For CBZ, NB, BA, and DMOB, the isocratic mobile phase consisted of water (pH 2.0, adjusted using phosphoric acid) and methanol (50:50, V/V%) at a flow rate of 1.0 mL/min, and the reference wavelengths were 286 nm, 264 nm, 230 nm, and 224 nm, respectively (Yin and Shang, 2020). For CAF, the eluents of water (pH 2.0, adjusted using phosphoric acid) and methanol (70:30 V/V%) were used at a flow rate of 1.0 mL/min, and the reference wavelength was 217 nm. Eluents of water (pH 2.0, adjusted using phosphoric acid) and methanol (70:30 V/V%) were used to measure IBP, and the reference wavelength was 220 nm. The concentrations of the selected bromo- and chloro-organic DBPs were determined according to the U.S. EPA Method 551.1 (APHA, 2017) by a gas chromatography (GC) system (Agilent 7890) equipped with an electron capture detector (ECD, from Agilent Technologies) and an HP-5MS fused silica capillary column (30 m × 0.25 mm, 0.25 µm, Agilent J&W). The concentrations of ClO_2^-, ClO_3^-,

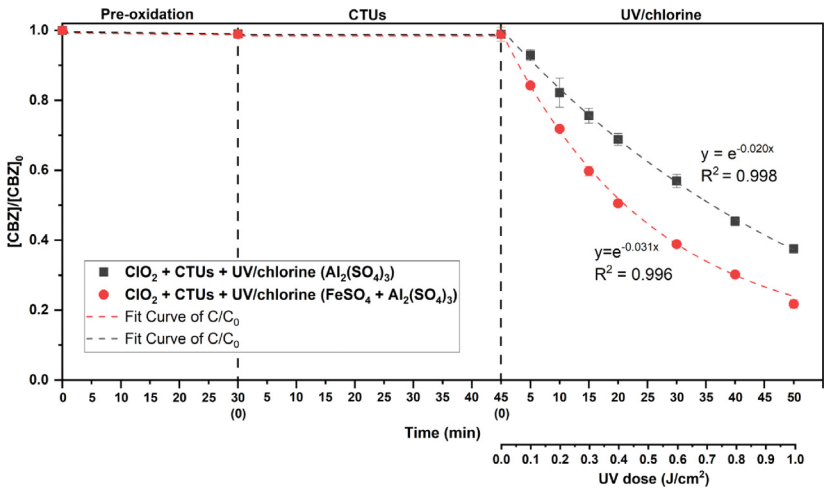

Fig. 2 – Degradation of CBZ in the ClO_2 pre-oxidation, CTUs, and UV/chlorine processes using $Al_2(SO_4)_3$ or the combination of $Al_2(SO_4)_3$ and $FeSO_4$ as the coagulant. Conditions: $[SRNOM]_0$ = 3.0 mg C/L, $[ClO_2]_0$ = 1.0 mg/L, pre-oxidation time = 30 min, $[Al_2(SO_4)_3]_0$ = 0.36 mmol/L as Al, $[Fe(II)]_0$ = 0.05 mmol/L, $[CBZ]_0$ = 2.0 μmol/L, $[chlorine]_0$ = 5.0 mg/L as Cl_2, [phosphate buffer] = 2.0 mmol/L, UV dose = 0–1000 mJ/cm^2, and pH = 6.5.

and Cl^-were quantified using an ion chromatography (IC, 940 Professional IC Vario, Metrohm). The concentrations of Fe(II) was determined by 1,10-phenanthroline method (Wang et al., 2010). UV-vis absorption spectra were determined using a 1-cm quartz cell on a spectrophotometer (UH5300, Hitachi). For electron paramagnetic resonance (EPR) measurements DMPO was immediately mixed with samples taken during the UV/chlorine process. EPR measurements were conducted at 9.85 GHz with a center field of 3508 G, a modulation frequency of 100 kHz, a sweep width of 80 G, a sweep time of 44.09 sec, a time constant of 0.01 msec, and a microwave power of 22.48 mW. The potential toxicity associated with the investigated chloro-organic DBPs was calculated by dividing the molar concentration of each DBP by their corresponding LC_{50} cytotoxicity (Appendix A Table S3) toward Chinese hamster ovary cells (total calculated cytotoxicity = $\Sigma([DBP]/LC_{50})$) (Chuang and Mitch, 2017; Cuthbertson et al., 2019; Zeng et al., 2016) (see details in Appendix A Text S2). Total organic carbon (TOC) was measured using a TOC analyzer (TOC-L series, Shimadzu).

2. Results and discussion

2.1. *Effects of Fe(II) addition on the degradation of CBZ*

The effect of Fe(II) addition on CBZ degradation in the proposed treatement train (ClO_2-CTUs-UV/chlorine) was firstly evaluated. Fig. 2 shows the time-dependent changes of CBZ concentration (C/C_0) in the three stages: pre-oxidation, CTUs, and post-UV/chlorine treatment. CBZ was barely degraded (<3%) in the ClO_2 pre-oxidation stage, in line with the reported low reactivity of CBZ towards ClO_2 (second-order rate constant $< 1.5 \times 10^{-2}$ (mol/L)$^{-1}$ sec^{-1}) (Gan et al., 2020). CBZ was not removed by CTUs either, no matter with or without Fe(II) addition. CBZ was rapidly degraded in the post-UV/chlorine process and the degradation followed pseudo-first-order kinetics. The degradation rate constant of CBZ was 0.02 min^{-1} in the UV/chlorine process without Fe(II) addition (in other words, using $Al_2(SO_4)_3$ only). Interestingly, the CBZ degradation rate constant increased by 55.0% to 0.03 min^{-1} by mixing 52.1 μmol/L of Fe(II) with $Al_2(SO_4)_3$ during CTUs. It should be noted that the residual ClO_2 and Fe(II) concentrations after CTUs were as low as < 0.05 mg/L as ClO_2 and < 0.5 mg/L as Fe, respectively. Supplementray tests indicated that 0.6 mg/L of Fe(II) had negligible impact on CBZ degradation in the UV/chlorine process under the experimental conditions (Appendix A Fig. S3). To verify whether the residual Fe(II)/Fe(III) species affected the measurement of the concentrations of free chlorine and ClO_2 by the DPD Colorimetric Method (4500-Cl G), the absorption spectra of the water samples with or without Fe(II) after the coagulation-sedimentation process were determined and show in Appendix A Fig. S4. The absorption spectra just slightly changed in the UV range of 200–600 nm with the addition of $FeSO_4$. The results suggested that the majority of the Fe(II)/Fe(III) species were settled down and removed after the coagulation-sedimentation process before the water goes into the post UV/chlorine process. Furthermore, the concentrations of free chlorine and ClO_2 residuals were determined using the DPD Colorimetric Method (4500-Cl G) in this study (APHA, 2017), which measured the absorbance of the samples at 515 nm. As shown in the spectra below, the absorbance of the sample containing the Fe(III)/Fe(II) species was rather low (0.003) at 515 nm. Therefore, the interference from the Fe(III)/Fe(II) species on the measurement of the concentrations of free chlorine and ClO_2 was anticipated to be negligible. The enhanced degradation of CBZ was thus hypothesized to be attributed to the increased concentrations of radicals (e.g., $HO^{\cdot}$, $Cl^{\cdot}$ and $ClO^{\cdot}$) in the UV/chlorine process with Fe(II) addition, because the added Fe(II) was anticipated to reduce the ClO_2^- formed from ClO_2 pre-oxidation before

it entered the UV/chlorine process (Eq. (1)) and alleviated the scavenging effects of ClO_2^- on the radicals (Zhao et al., 2021).

Additional experiments were conducted to investigate whether the Fe(II) addition could enhance the degradation of different micropollutants other than carbamazepine and explain the associated mechanisms. Two more micropollutants (ibuprofen and caffeine) were selected for investigation, because (1) both compounds are frequently detected in surface waters, and (2) they cannot be degraded by chlorine nor chlorine dioxide, but are reactive towards $HO^{\cdot}$ and reactive chlorine species (Huber et al., 2005; Lee and von Gunten, 2010; Xiang et al., 2016). As shown in Appendix A Fig. S2, the degradation rate constants of ibuprofen and caffeine were 0.013 and 0.009 min^{-1}, respectively, in the UV/chlorine process without Fe(II) addition. With the addition of 52.1 μmol/L of Fe(II), the degradation rate constants of ibuprofen and caffeine increased by 98.4% and 121.1%, respectively. The increase of the degradation rate constants of the two micropollutants was supported by the increased radical concentration with Fe(II) addition, as discussed in Section 2.2. The higher enhancement to caffeine than ibuprofen was because (1) the degradation of caffeine in the UV/chlorine process was predominantly contributed by $ClO^{\cdot}$ (Guo et al., 2018, 2017), and (2) the Fe(II) addition increased the concentration of $ClO^{\cdot}$ more significantly than other radicals (see details in Section 2.2).

The results suggested that the Fe(II) addition not only enhanced the degradation of carbamazepine, but also worked to ibuprofen and caffeine, and it is expected to enhance the degradation of many other micropollutants that are reactive towards radicals ($HO^{\cdot}$, $Cl^{\cdot}$, and $ClO^{\cdot}$).

2.2. *Effects of Fe(II) addition on radical concentrations in the UV/chlorine process*

To verify the above hypothesis that Fe(II) addition increased the radical concentrations, the steady-state concentrations of $HO^{\cdot}$ ($[HO^{\cdot}]_{ss}$), $Cl^{\cdot}$ ($[Cl^{\cdot}]_{ss}$), and $ClO^{\cdot}$ ($[ClO^{\cdot}]_{ss}$) in the post-UV/chlorine process (after ClO_2 pre-oxidation and CTUs treatment) were experimentally determined using three probe compounds (NB, BA, and DMOB) (Yin et al., 2019). NB was used as a probe compound to determine $[HO^{\cdot}]_{ss}$, since it reacts rapidly with $HO^{\cdot}$ but barely reacts with reactive chlorine species (i.e., $Cl^{\cdot}$ and $ClO^{\cdot}$, Appendix A Table S1) (Bulman et al., 2019). BA is highly reactive towards $HO^{\cdot}$ and $Cl^{\cdot}$, but less reactive towards $ClO^{\cdot}$ (Appendix A Table S1) (Alfassi et al., 1987; Buxton et al., 1988; Mártire et al., 2001; Yin et al., 2018). It was thus used together with the concentration of $HO^{\cdot}$ determined using NB, to calculate the $[Cl^{\cdot}]_{ss}$. DMOB which is reactive towards $HO^{\cdot}$, $Cl^{\cdot}$, and $ClO^{\cdot}$ (Appendix A Table S1) (Alfassi et al., 1989; Alfassi et al., 1987; O'Nelll et al., 1975), was used, together with the data collected using NB and BA, to determine the $[ClO^{\cdot}]_{ss}$. The detailed procedures and principles of determination of radical concentrations are shown in Appendix A Text S1.

Fig. 3, without Fe(II) addition, $[HO^{\cdot}]_{ss}$ and $[Cl^{\cdot}]_{ss}$ in the post-UV/chlorine process were determined to be $(2.79\pm0.10) \times 10^{-14}$ mol/L and $(6.80\pm0.06) \times 10^{-15}$ mol/L, respectively, while $[ClO^{\cdot}]_{ss}$ was not detectable. With the addition of 52.1 μmol/L of Fe(II) in the CTUs, $[HO^{\cdot}]_{ss}$ and $[Cl^{\cdot}]_{ss}$ increased by 41.6% and 4.4%, respectively. $[ClO^{\cdot}]_{ss}$ also increased and became

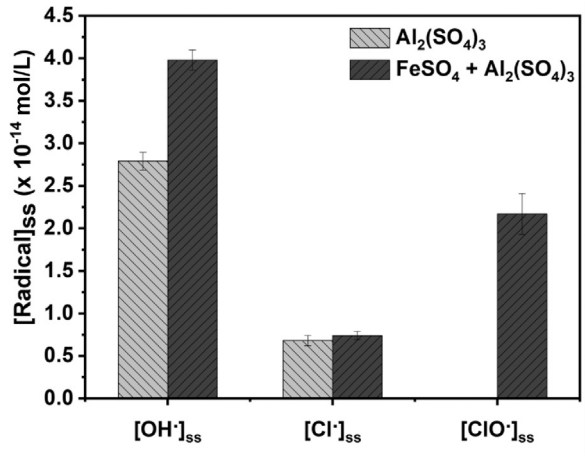

Fig. 3 – Steady-state concentrations of $HO^{\cdot}$, $Cl^{\cdot}$, and $ClO^{\cdot}$ in the UV/chlorine process using $Al_2(SO_4)_3$ or the combination of $Al_2(SO_4)_3$ and $FeSO_4$ as the coagulant. Conditions: $[SRNOM]_0$ = 3.0 mg C/L, $[ClO_2]_0$ = 1.0 mg/L, pre-oxidation time = 30 min, $[Al_2(SO_4)_3]_0$ = 0.36 mmol/L as Al, $[Fe(II)]_0$ = 0.05 mmol/L, $[CBZ]_0 = [NB]_0 = [BA]_0 = [DMOB]_0$ = 2.0 μmol/L, $[chlorine]_0$ = 5.0 mg/L, [phosphate buffer] = 2.0 mmol/L, and UV dose = 1000 mJ/cm^2, and pH = 6.5.

detectable, with a concentration of $(2.17\pm0.24) \times 10^{-14}$ mol/L. The results clearly demonstrated that the concentrations of radicals (especially $HO^{\cdot}$ and $ClO^{\cdot}$) in the post-UV/chlorine process were significantly increased by adding micromolar-level Fe(II) in the coagulants, compared to the case using $Al_2(SO_4)_3$ alone for coagulation. The above results supported the experimental observation in Fig. 2 that the CBZ degradation increased with Fe(II) addition. The increased radical concentrations were likely due to the reduction of ClO_2^- by Fe(II). One evidence to support this hypothesis was that the Fe(II) addition showed more significant impact on $ClO^{\cdot}$ and $HO^{\cdot}$ compared to $Cl^{\cdot}$ (Fig. 3), which was consistent with the previous finding that ClO_2^- exhibited more significant scavenging effect on $ClO^{\cdot}$ and $HO^{\cdot}$ than $Cl^{\cdot}$ in the UV/chlorine process (Zhao et al., 2021). Additional experiments using EPR spectroscopy to enhance the interpretation of the radical chemistry were also carried out. As presented in Appendix A Fig. S5, the EPR spectra showed the typical DMPO-$HO^{\cdot}$ adduct (as a 1:2:2:1 quartet) and the DMPOX signal (the oxidized form of DMPO) (Liu et al., 2016). The DMPO-$HO^{\cdot}$ signal was stronger with Fe(II) addition, indicating that $HO^{\cdot}$ were present in higher concentrations when Fe(II) was added. Apart from $HO^{\cdot}$, the EPR cannot detect and differentiate $ClO^{\cdot}$ and $Cl^{\cdot}$, because (1) the DMPOX peaks can form by single electron transfers (SET) (Liu et al., 2016; Wang et al., 2019), and (2) SET mechanisms can be initiated by both $ClO^{\cdot}$ and $Cl^{\cdot}$.

2.3. *Effects of Fe(II) addition on ClO_2^- and ClO_3^- formation in the integrated process*

To verify the hypothesis that Fe(II) addition reduced the ClO_2^- concentration, experiments were conducted to quantify the concentrations of ClO_2^- in the integrated process (ClO_2-CTUs-

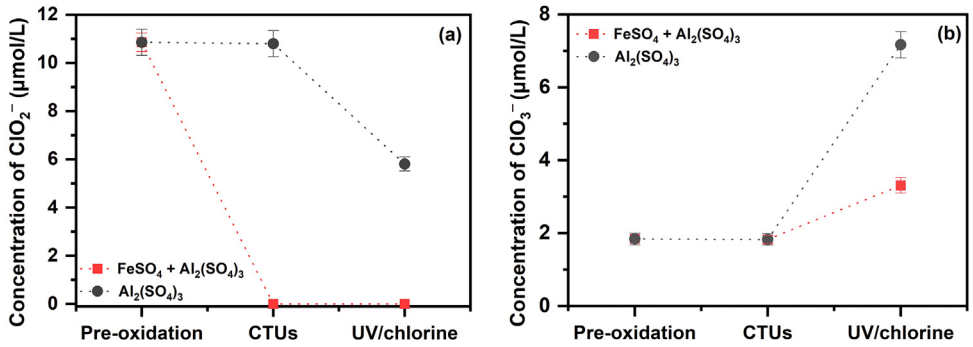

Fig. 4 – Formation of (a) ClO_2^- and (b) ClO_3^- after each step in the integrated process using $Al_2(SO_4)_3$ combination of $Al_2(SO_4)_3$ and $FeSO_4$ as coagulant. Conditions: $[SRNOM]_0$ = 3.0 mg C/L, $[Al_2(SO_4)_3]_0$ = 0.36 mmol/L as Al, $[Fe(II)]_0$ = 0.05 mmol/L as Fe(II), $[ClO_2]_0$ = 1.0 mg/L, pre-oxidation time = 30 min, $[chlorine]_0$ = 5.0 mg/L, [phosphate buffer] = 2.0 mmol/L, UV dose = 1000 mJ/cm^2, and pH = 6.5.

UV/chlorine). As shown in Fig. 4a, 10.8±0.4 μmol/L of ClO_2^- was formed from pre-oxidation by 1.0 mg/L of ClO_2 (14.8 μmol/L) for 30 min. The molar yield of ClO_2^- was calculated to be 72.3%, in accordance with the reported values (30%–70%) (Gan et al., 2020; Yang et al., 2013b). The formed ClO_2^- was barely removed by the subsequent CTUs when only $Al_2(SO_4)_3$ was used. In the following UV/chlorine process, ClO_2^- was reduced by 46.4% to 5.8±0.3 μmol/L. The reduction was mainly attributed to the oxidation of ClO_2^- to ClO_3^- by the radicals in the UV/chlorine process (Zhao et al., 2021). As shown in Appendix A Fig. S6, when 52.1 μmol/L of Fe(II) was added in the coagulant, the 10.8±0.4 μmol/L of ClO_2^- formed from ClO_2 pre-oxidation was completely reduced during the CTUs, while the concentration of chloride ion (Cl^-) increased from 5.9±0.4 μmol/L to 16.6±0.5 μmol/L. A good mass balance was achieved (99.1%), suggesting that nearly all the ClO_2^- was reduced to Cl^-. Moreover, no ClO_2^- could be detected after the UV/chlorine treatment. The results clearly demonstrated that the addition of Fe(II) effectively eliminated ClO_2^- formed from pre-oxidation and controlled the ClO_2^- in the integrated process. The results also supported the previous hypothesis that the increased radical concentrations and CBZ degradation were attributed to the reduction of ClO_2^- by Fe(II) in the CTUs.

ClO_3^- is the oxidation product of ClO_2^- and a DBP of health concern (Couri et al., 1982). Its concentrations in the integrated process were also monitored. As shown in Fig. 4b, 1.8±0.2 μmol/L of ClO_3^- was formed from pre-oxidation by 1 mg/L of ClO_2 (14.8 μmol/L) for 30 min, with a molar yield of 12.3%, in accordance with the reported values (~10%) (Gan et al., 2020; Yang et al., 2013b). CTUs with $Al_2(SO_4)_3$ barely removed ClO_3^-. The ClO_3^- concentration increased by 289.7% to 7.2±0.4 μmol/L (0.60 mg/L) after the UV/chlorine treatment. The increase of ClO_3^- concentration was attributed to the oxidation of ClO_2^- by radicals and the photolysis of chlorine (Rao et al., 2012; Zhao et al., 2021). Unlike ClO_2^-, ClO_3^- was just slightly reduced when Fe(II) was added into the coagulant (Fig. 4b). This was consistent with the much lower reactivity of Fe(II) towards ClO_3^- than ClO_2^- (Gonce and Voudrias, 1994). The ClO_3^- concentration increased by 79.9% to 3.3±0.2 μmol/L (0.28 mg/L) after the UV/chlorine treatment, mainly due to the chlorine photolysis. Compared to the case without Fe(II) addition, the increase of ClO_3^- concentration from CTUs to the UV/chlorine treatment was less significant with Fe(II) addition (79.9% *vs.* 289.7%). Moreover, compared to the case without Fe(II) addition, the final concentration of ClO_3^- in the integrated process with Fe(II) addition was 72.7% lower (0.28 mg/L *vs.* 0.60 mg/L). Notably, the final concentration of ClO_3^- in the integrated process with Fe(II) addition was lower than the WHO drinking water standard (0.7 mg/L) (WHO, 2017).

The above results suggested that the Fe(II) addition reduced ClO_2^- concentration, increased the radical concentrations and micropollutant degradation in the UV/chlorine process, and reduced the final concentration of ClO_3^- as well as the detrimental health impacts of the proposed advanced treatment train.

2.4. *Effects of different Fe(II) concentrations on carbamazepine degradation*

Supplementary experiments were conducted to investigate the effect of gradient Fe(II) concentration on the removal of micropollutants, chlorite and chlorate in the integrated process (ClO_2-CTUs-UV/chlorine). Previously, Fe(II) was dosed at 52.1 μmol/L to achieve the near-stoichiometric reduction of ClO_2^- ($4Fe^{2+} + ClO_2^- \rightleftharpoons 4Fe(OH)_3 + 4e^- + Cl^- + 8H^+$). Additionally, Fe(II) was dosed at another two concentrations at 21.7 μmol/L (50% lower than the stoichiometric dosage) and 86.8 μmol/L (50% higher than the stoichiometric dosage). As shown in the Fig. 5, increasing the Fe(II) dosage from 21.7 to 52.1 μmol/L increased the CBZ degradation rate constant by 24.0%, from 0.025 min^{-1} to 0.031 min^{-1}. While further increasing the Fe(II) dosage from 52.1 to 86.8 μmol/L decreased the CBZ degradation rate constant by 45.2% to 0.017 min^{-1}. The results suggested that the CBZ degradation efficiency increased with Fe(II) dosage when the dosage was near-stoichiometric dosage (52.1 μmol/L), while excessive (over the stoichiometric dosage) Fe(II) had inhibitory effect on CBZ degradation. To explain the trend observed, the concentrations of the radicals were determined at the three Fe(II) dosages and the results were shown in Appendix A Fig. S8. Increasing the Fe(II) dosage from 21.7 to 52.1 μmol/L increased the $[HO^{\cdot}]_{ss}$ and $[Cl^{\cdot}]_{ss}$ by 20.6% and 8.8% from (3.31±0.24) × 10^{-14} to (3.98±0.12) × 10^{-14}

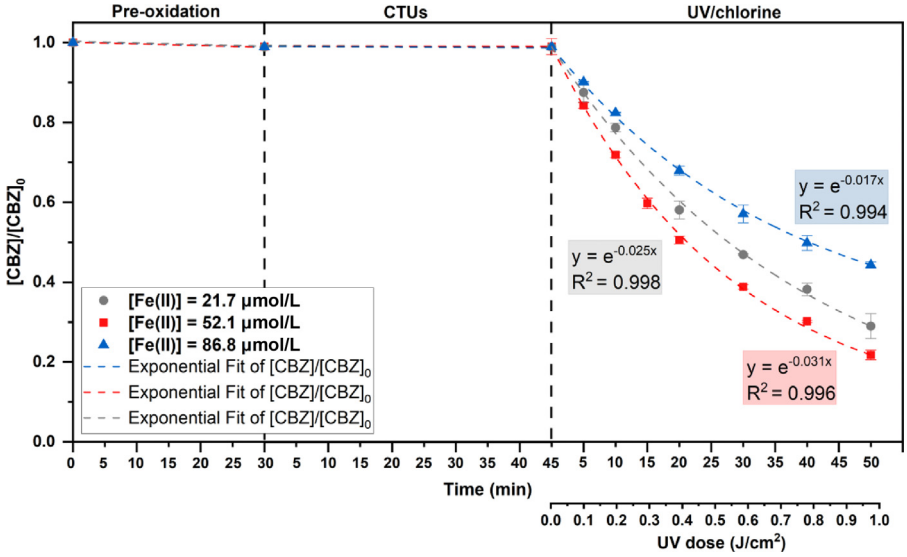

Fig. 5 – Degradation of CBZ in the ClO_2 pre-oxidation, CTUs, and UV/chlorine processes using the combination of $Al_2(SO_4)_3$ and different concentrations of $FeSO_4$. Conditions: $[SRNOM]_0$ = 3.0 mg C/L, $[ClO_2]_0$ = 1.0 mg/L, pre-oxidation time = 30 min, $[coagulant]_0$ = 0.36 mmol/L as Al, $[Fe(II)]_0$ = 0.05, 0.02, and 0.09 mmol/L, $[CBZ]_0$ = 2.0 μmol/L, $[chlorine]_0$ = 5.0 mg/L as Cl_2, [phosphate buffer] = 2.0 mmol/L, UV dose = 0–1000 mJ/cm^2, and pH = 6.5.

mol/L, and from (6.77±0.02) × 10^{-15} to (7.42±0.05) × 10^{-15} mol/L, respectively. $ClO^{\cdot}$ was undetectable at a Fe(II) dosage of 21.7 but became detectable at a Fe(II) dosage of 52.1 μmol/L. While further increasing the Fe(II) dosage from 52.1 to 86.8 μmol/L decreased the $[HO^{\cdot}]_{ss}$, $[Cl^{\cdot}]_{ss}$, and $[ClO^{\cdot}]_{ss}$ by 40.5%, 46.0%, and 21.2%, respectively. The effect of Fe(II) dosage on the radical concentrations was consistent with its effect on CBZ degradation. The lower radical concentration at 21.7 than 52.1 μmol/L was because ClO_2^- was not completely scavenged by Fe(II), entered the UV/chlorine process, and scavenged the radicals formed. The lower radical concentration at 86.8 than 52.1 μmol/L was because the excessive Fe(II) with a reductive nature consumed the radicals formed in the UV/chlorine process.

Experiments were also conducted to determine the ClO_2^- and ClO_3^- concentration formed at different Fe(II) dosages. As shown in the Appendix A Fig. S7a, when 21.7 μmol/L of Fe(II) was dosed, the ClO_2^- concentrations were 10.8, 5.1, and 1.2 μmol/L after pre-oxidation, CTUs, and the UV/chlorine stage, respectively. By increasing the Fe(II) dosage to 52.1 and 86.8 μmol/L, ClO_2^- was undetectable after CTUs and the UV/chlorine process. The results suggested that the ClO_2^- removal efficiency increased with increasing Fe(II) dosage. ClO_3^-, the oxidation product of ClO_2^-, slightly changed during pre-oxidation and CTUs in the three cases. The ClO_3^- concentration in the UV/chlorine process was 4.3 μmol/L at a Fe(II) dosage of 21.7 μmol/L. Increasing the Fe(II) dosage from 21.7 to 52.1 μmol/L decreased the ClO_3^- concentration by 23.3% to 3.3 μmol/L. Further increasing the Fe(II) dosage from 52.1 to 86.8 μmol/L barely changed the ClO_3^- concentration (Appendix A Fig. S7b). The results on ClO_3^- formation were consistent with that on ClO_2^- formation, as higher ClO_2^- residual resulted in higher ClO_3^- formation.

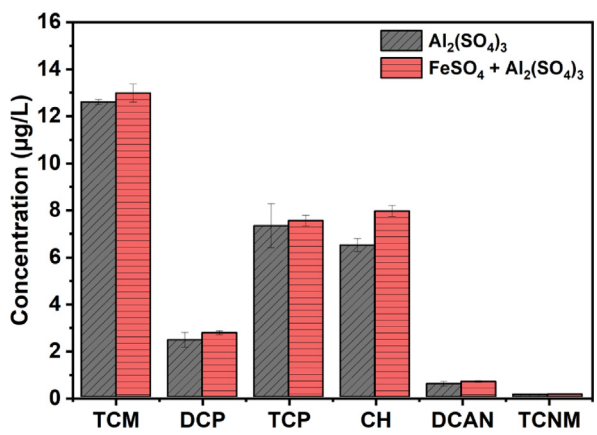

Fig. 6 – Formation of chloro-organic DBP in the integrated process using $Al_2(SO_4)_3$ or the combination of $Al_2(SO_4)_3$ and $FeSO_4$ as the coagulant. Conditions: $[SRNOM]_0$ = 3.0 mg C/L, [coagulant] = 0.36 mmol/L as Al, $[Fe(II)]_0$ = 0.05 mmol/L, $[ClO_2]_0$ = 1.0 mg/L, $[chlorine]_0$ = 5.0 mg/L, [phosphate buffer] = 2.0 mmol/L, pre-oxidation time = 30 min, and UV dose = 1000 mJ/cm^2, and pH = 6.5.

2.5. *Effects of Fe(II) addition on chloro-organic DBP formation in the integrated process*

The effect of Fe(II) addition on the formation of chloro-organic DBPs in the integrated process (ClO_2-CTUs-UV/chlorine) was also evaluated Fig. 6. shows the concentrations of the six selected chloro-organic DBPs (TCM, DCP, TCP, CH, DCAN, and TCNM) in the integrated process with or without Fe(II) addition. Among the six selected DBPs, the effect of Fe(II) addition

on the formation of TCM, TCP, DCAN, and TCNM was statistically insignificant ($p > 0.05$). Fe(II) addition slightly increased the concentrations of CH and DCP by 22.6% and 12.5%, respectively ($p < 0.05$). The slight increase of DBP concentrations with Fe(II) addition was likely attributed to the increased concentrations of radicals in the UV/chlorine process after ClO_2^- reduction by Fe(II), as discussed in Section 2.2. The radicals (e.g., $Cl^{\cdot}$) were reported to undergo Cl-substitution and Cl-addition reactions with NOM to form chloro-organic DBPs (Wang et al., 2017; Xiang et al., 2016). Notably, the concentrations of the selected DBPs were well below the regulatory limits, e.g., TCM and DCAN concentration was lower than the WHO standard (2017) (300 μg/L and 20 μg/L, respectively). Additional experiments were conducted to determine the TOC concentrations after each step of the integrated process with or without Fe(II) addition. As shown in the Appendix A Fig. S9, the TOC after the CTUs decreased from 2.86±0.11 to 1.49±0.27 mg/L with the addition of 52.1 μmol/L of Fe(II). The decrease of TOC was more significant at higher Fe(II) dosages. The reduction of TOC was likely due to the enhanced coagulation assisted by the Fe species in the system. The normalized DBP concentration over the TOC concentration (μg DBP/mg TOC) was calculated and the results are shown in Appendix A Table S2. The TOC-normalized DBP concentrations were higher with the addition of Fe(II). The increases were mainly attributed to the increased radical generated in the UV/chlorine process, because the added Fe(II) effectively reduced ClO_2^- and eliminated its scavenging effects on the radicals. The byproduct-associated toxicity of the treated water with or without Fe(II) dosing was calculated by using the toxicity weighting method (Chuang and Mitch, 2017; Cuthbertson et al., 2019; Zeng et al., 2016) (see details in Appendix A Text S2). As shown in the Appendix A Fig. S10a, the organic byproduct associated toxicity of the water treated by the integrated process increased slightly by 17.6% with Fe(II) dosing, compared to the case without Fe(II) dosing. As discussed above, the Fe(II) dosing reduced ClO_2^-, resulting in an increased radical concentrations, and slightly increased the chloro-organic byproduct formation. Nonetheless, even though the organic byproducts and their associated toxicity were increased slightly by Fe(II) dosing, the inorganic byproduct (ClO_2^- and ClO_3^-) concentrations were decreased significantly. As shown in Appendix A Fig. S10b, the inorganic byproduct associated toxicity decreased by 72.3% with Fe(II) dosing, compared to the case without Fe(II) dosing. The reduction percentage (72.3%) of the inorganic byproduct associated toxicity was 4.1 times higher than the increase percentage (17.6%) of the organic byproduct associated toxicity. However, it is uncertain whether the overall toxicity of the treated water will be decreased or not, because the organic- and inorganic byproduct associated toxicity were calculated in different ways, i.e., organic byproducts have the LC_{50} values available in literature while the inorganic byproducts do not. Following the literature, the values of 50% lifetime excess non-cancer risk ($LENCR_{50}$, in molar units) available for ClO_2^- and ClO_3^- were used to calculate the corresponding associated toxicity (see details in Appendix A Text S2) (Chuang and Mitch, 2017). Moreover, some previous studies reported that the inorganic- and chloro-organic byproducts may show a synergistic toxicity effect rather than the additive relationship (Han and Zhang, 2018). The above results suggested that the addition of Fe(II) enabled simultaneous enhancement of micropollutant degradation and reduction to ClO_2^- and ClO_3^-, with minor impact on the formation of chloro-organic DBPs in the proposed advanced drinking water treatment train.

Previous works indicated the enhancement of bromo-organic DBPs formation after ClO_2 pre-oxidation (Yang et al., 2013a). Therefore, bromo-organic DBPs were also investigated (Appendix A Fig. S11) and the results are discussed in Appendix A Text S3.

3. Conclusions

This study evaluated the effects of adding micromolar levels of Fe(II) in the coagulants on the micropollutant degradation and byproduct control in an advanced drinking water treatment train comprising ClO_2 pre-oxidation, CTUs, and UV/chlorine AOP. The addition of Fe(II) effectively eliminated the ClO_2^- generated from ClO_2 pre-oxidation, increased the radical concentrations ($OH^{\cdot}$ and $ClO^{\cdot}$ mainly), enhanced micropollutant degradation, and decreased ClO_2^- and ClO_3^- concentrations in the treatment train, while its impact on the formation of chloro-organic DBPs was rather minor. The findings in this study provided fundamental evidences to support a promising advanced treatment train to improve drinking water quality and safety.

Acknowledgement

This study was supported by the Hong Kong Innovation and Technology Fund (No. GHP/010/18GD), the National Natural Science Foundation of China (No. 21876210), and the Hong Kong Research Grants Council (No. T21-604/19-R). The work was also partially supported by a fellowship award from the Research Grants Council of the Hong Kong Special Administrative Region, China (No. HKUST PDFS2021-6S05).

Appendix A Supplementary data

Supplementary material associated with this article can be found, in the online version, at doi:10.1016/j.jes.2022.03.022.

REFERENCES

Aghdam, E., Xiang, Y., Sun, J., Shang, C., Yang, X., Fang, J., 2017. DBP formation from degradation of DEET and ibuprofen by UV/chlorine process and subsequent post-chlorination. J. Environ. Sci. 58, 146–154. doi:10.1016/j.jes.2017.06.014.

Alfassi, Z.B., Huie, R.E., Mosseri, S., Neta, P., 1987. Kinetics of one-electron oxidation by the cyanate radical. J. Phys. Chem. 91, 3888–3891. doi:10.1021/j100298a031.

Alfassi, Z.B., Mosseri, S., Neta, P., 1989. Reactivities of chlorine atoms and peroxyl radicals formed in the radiolysis of dichloromethane. J. Phys. Chem. 93, 1380–1385. doi:10.1021/j100341a040.

APHA, 2017. Standard Methods for the Examination of Water and Wastewater, 23rd ed. AWWA, Washington DC.

Behin, J., Akbari, A., Mahmoudi, M., Khajeh, M., 2017. Sodium hypochlorite as an alternative to hydrogen peroxide in Fenton process for industrial scale. Water Res 121, 120–128. doi:10.1016/j.watres.2017.05.015.

Benotti, M.J., Trenholm, R.A., Vanderford, B.J., Holady, J.C., Stanford, B.D., Snyder, S.A., 2009. Pharmaceuticals and endocrine disrupting compounds in U.S. Drinking water. Environ. Sci. Technol. 43, 597–603. doi:10.1021/es801845a.

Bolton, J.R., Linden, K.G., 2003. Standardization of methods for fluence (UV Dose) determination in bench-scale UV experiments. J. Environ. Eng. 129, 209–215. doi:10.1061/(ASCE)0733-9372(2003)129:3(209).

Buxton, G.V, Greenstock, C.L., Helman, W.P., Ross, A.B., 1988. Critical review of rate constants for reactions of hydrated electrons, hydrogen atoms and hydroxyl radicals (·OH/·O−) in aqueous solution. J. Phys. Chem. Ref. Data 17, 513–886. doi:10.1063/1.555805.

Chuang, Y.H., Mitch, W.A., 2017. Effect of ozonation and biological activated carbon treatment of wastewater effluents on formation of n-nitrosamines and halogenated disinfection byproducts. Environ. Sci. Technol. 51, 2329–2338. doi:10.1021/acs.est.6b04693.

Couri, D., Abdel-Rahman, M.S., Bull, R.J., 1982. Toxicological effects of chlorine dioxide, chlorite and chlorate. Environ. Health Perspect. 46, 13–17. doi:10.1289/ehp.824613.

Cuthbertson, A.A., Kimura, S.Y., Liberatore, H.K., Summers, R.S., Knappe, D.R.U., Stanford, B.D., et al., 2019. Does granular activated carbon with chlorination produce safer drinking water? from disinfection byproducts and total organic halogen to calculated toxicity. Environ. Sci. Technol. 53, 5987–5999. doi:10.1021/acs.est.9b00023.

Daughton, C.G., 2004. Non-regulated water contaminants: emerging research. Environ. Impact Assess. Rev. 24, 711–732. doi:10.1016/j.eiar.2004.06.003.

Dixon, K.L., Lee, R.G., 1991. The effect of sulfur-based reducing agents and GAC filtration on chlorine dioxide by-products. J. Am. Water Works Assoc. 83, 48–55. doi:10.1002/j.1551-8833.1991.tb07146.x.

Fan, M., Yang, X., Kong, Q., Lei, Y., Zhang, X., Aghdam, E., et al., 2022. Sequential ClO_2-UV/chlorine process for micropollutant removal and disinfection byproduct control. Sci. Total Environ. 806, 150354. doi:10.1016/j.scitotenv.2021.150354.

Furman, C.S., Margerum, D.W., 1998. Mechanism of chlorine dioxide and chlorate ion formation from the reaction of hypobromous acid and chlorite ion. Inorg. Chem. 37, 4321–4327. doi:10.1021/ic980262q.

Gan, W., Ge, Y., Zhong, Y., Yang, X., 2020. The reactions of chlorine dioxide with inorganic and organic compounds in water treatment: kinetics and mechanisms. Environ. Sci. Water Res. Technol. 6, 2287–2312. doi:10.1039/D0EW00231C.

Gan, W., Huang, S., Ge, Y., Bond, T., Westerhoff, P., Zhai, J., et al., 2019. Chlorite formation during ClO_2 oxidation of model compounds having various functional groups and humic substances. Water Res 159, 348–357. doi:10.1016/j.watres.2019.05.020.

Gonce, N., Voudrias, E.A., 1994. Removal of chlorite and chlorate ions from water using granular activated carbon. Water Res 28, 1059–1069. doi:10.1016/0043-1354(94)90191-0.

Guo, K., Wu, Z., Shang, C., Yao, B., Hou, S., Yang, X., et al., 2017. Radical chemistry and structural relationships of PPCP degradation by UV/chlorine treatment in simulated drinking water. Environ. Sci. Technol. 51, 10431–10439. doi:10.1021/acs.est.7b02059.

Guo, K., Wu, Z., Yan, S., Yao, B., Song, W., Hua, Z., et al., 2018. Comparison of the UV/chlorine and UV/H2O2 processes in the degradation of PPCPs in simulated drinking water and wastewater: Kinetics, radical mechanism and energy requirements. Water Res 147, 184–194. doi:10.1016/j.watres.2018.08.048.

Han, J., Zhang, X., 2018. Evaluating the comparative toxicity of DBP mixtures from different disinfection scenarios: a new approach by combining freeze-drying or rotoevaporation with a marine polychaete bioassay. Environ. Sci. Technol. 52, 10552–10561. doi:10.1021/acs.est.8b02054.

Henderson, R., Carlson, K., Gregory, D., 2001. The impact of ferrous ion reduction of chlorite ion on drinking water process performance. Water Res 35, 4464–4473. doi:10.1016/S0043-1354(01)00172-5.

Hu, J., Chu, W., Sui, M., Xu, B., Gao, N., Ding, S., 2018. Comparison of drinking water treatment processes combinations for the minimization of subsequent disinfection by-products formation during chlorination and chloramination. Chem. Eng. J. 335, 352–361. doi:10.1016/j.cej.2017.10.144.

Huber, M.M., Korhonen, S., Ternes, T.A., von Gunten, U., 2005. Oxidation of pharmaceuticals during water treatment with chlorine dioxide. Water Res 39, 3607–3617. doi:10.1016/j.watres.2005.05.040.

Hurst, G.H., Knocke, W.R., 1997. Evaluating ferrous iron for chlorite ion removal. J. Am. Water Works Assoc. 89, 98–105. doi:10.1002/j.1551-8833.1997.tb08280.x.

Iatrou, A., Knocke, W.R., 1992. Removing chlorite by the addition of ferrous iron. J. Am. Water Works Assoc. 84, 63–68. doi:10.1002/j.1551-8833.1992.tb05883.x.

Kim, D., Ates, N., Kaplan Bekaroglu, S.S., Selbes, M., Karanfil, T., 2017. Impact of combining chlorine dioxide and chlorine on DBP formation in simulated indoor swimming pools. J. Environ. Sci. 58, 155–162. doi:10.1016/j.jes.2017.04.020.

Lee, Y., von Gunten, U., 2010. Oxidative transformation of micropollutants during municipal wastewater treatment: Comparison of kinetic aspects of selective (chlorine, chlorine dioxide, ferrateVI, and ozone) and non-selective oxidants (hydroxyl radical). Water Res doi:10.1016/j.watres.2009.11.045.

Liu, L.D., Wang, W.M., Liu, L., Yu, B., Zhang, Y.X., Wu, X.Q., et al., 2016. Catalytic activities of dissolved and Sch-immobilized Mo in H2O2 decomposition: Implications for phenol oxidation under acidic conditions. Appl. Catal. B Environ. 185, 371–377. doi:10.1016/j.apcatb.2015.12.010.

Liu, W., Zhang, Z., Yang, X., Xu, Y., Liang, Y., 2012. Effects of UV irradiation and UV/chlorine co-exposure on natural organic matter in water. Sci. Total Environ. 414, 576–584. doi:10.1016/j.scitotenv.2011.11.031.

Mártire, D.O., Rosso, J.A., Bertolotti, S., Carrillo Le Roux, G., Braun, A.M., Gonzalez, M.C., 2001. Kinetic study of the reactions of chlorine atoms and $Cl_2^{\cdot-}$ radical anions in aqueous solutions. II. Toluene, benzoic acid, and chlorobenzene. J. Phys. Chem. A 105, 5385–5392. doi:10.1021/jp004630z.

O'Neill, P., Steenken, S., Schulte-Frohlinde, D., 1975. Formation of radical cations of methoxylated benzenes by reaction with OH radicals, Ti^{2+}, Ag^{2+}, and $SO_4^{\cdot-}$ in aqueous solution. An optical and conductometric pulse radiolysis and in situ radiolysis electron spin resonance study. J. Phys. Chem. 79, 2773–2779. doi:10.1021/j100592a013.

Pai, C.W., Leong, D., Chen, C.Y., Wang, G.S., 2020. Occurrences of pharmaceuticals and personal care products in the drinking water of Taiwan and their removal in conventional water treatment processes. Chemosphere 256, 127002. doi:10.1016/j.chemosphere.2020.127002.

Pan, Y., Cheng, S., Yang, X., Ren, J., Fang, J., Shang, C., et al., 2017. UV/chlorine treatment of carbamazepine: Transformation products and their formation kinetics. Water Res 116, 254–265. doi:10.1016/j.watres.2017.03.033.

Qin, L., Lin, Y.L., Xu, B., Hu, C.Y., Tian, F.X., Zhang, T.Y., et al., 2014. Kinetic models and pathways of ronidazole degradation by

chlorination, UV irradiation and UV/chlorine processes. Water Res 65, 271–281. doi:10.1016/j.watres.2014.07.041.
Rao, B., Estrada, N., McGee, S., Mangold, J., Gu, B., Jackson, W.A., 2012. Perchlorate production by photodecomposition of aqueous chlorine solutions. Environ. Sci. Technol. 46, 11635–11643. doi:10.1021/es3015277.
Rougé, V., Allard, S., Croué, J.P., Von Gunten, U., 2018. *In situ* formation of free chlorine during ClO_2 Treatment: Implications on the formation of disinfection byproducts. Environ. Sci. Technol. doi:10.1021/acs.est.8b04415.
Rougé, V., Von Gunten, U., Lafont De Sentenac, M., Massi, M., Wright, P.J., Croué, J.P., et al., 2020. Comparison of the impact of ozone, chlorine dioxide, ferrate and permanganate pre-oxidation on organic disinfection byproduct formation during post-chlorination. Environ. Sci. Water Res. Technol. doi:10.1039/d0ew00411a.
Ruan, X., Xiang, Y., Shang, C., Cheng, S., Liu, J., Hao, Z., et al., 2021. Molecular characterization of transformation and halogenation of natural organic matter during the UV/chlorine AOP using FT-ICR mass spectrometry. J. Environ. Sci. 102, 24–36. doi:10.1016/j.jes.2020.08.028.
Sichel, C., Garcia, C., Andre, K., 2011. Feasibility studies: UV/chlorine advanced oxidation treatment for the removal of emerging contaminants. Water Res 45, 6371–6380. doi:10.1016/j.watres.2011.09.025.
Wang, H., Shen, Y., Lou, Z., Zhu, N., Yuan, H., Liu, C., 2019. Hydroxyl radicals and reactive chlorine species generation via E+-ozonation process and their contribution for concentrated leachate disposal. Chem. Eng. J. 360, 721–727. doi:10.1016/j.cej.2018.11.213.
Wang, S., Wang, H., Liu, Y., Fu, Y., 2020. Effective degradation of sulfamethoxazole with Fe^{2+}-zeolite/peracetic acid. Sep. Purif. Technol. 233, 115973. doi:10.1016/j.seppur.2019.115973.
Wang, W.L., Wu, Q.Y., Huang, N., Wang, T., Hu, H.Y., 2016. Synergistic effect between UV and chlorine (UV/chlorine) on the degradation of carbamazepine: Influence factors and radical species. Water Res 98, 190–198. doi:10.1016/j.watres.2016.04.015.
Wang, W.L., Zhang, X., Wu, Q.Y., Du, Y., Hu, H.Y., 2017. Degradation of natural organic matter by UV/chlorine oxidation: Molecular decomposition, formation of oxidation byproducts and cytotoxicity. Water Res 124, 251–258. doi:10.1016/j.watres.2017.07.029.
Wang, Z., Chen, X., Ji, H., Ma, W., Chen, C., Zhao, J., 2010. Photochemical cycling of iron mediated by dicarboxylates: special effect of malonate. Environ. Sci. Technol. 44, 263–268. doi:10.1021/es901956x.
WHO, 2017. Guidelines for drinking water quality, 4th ed.
Xiang, Y., Fang, J., Shang, C., 2016. Kinetics and pathways of ibuprofen degradation by the UV/chlorine advanced oxidation process. Water Res 90, 301–308. doi:10.1016/j.watres.2015.11.069.
Yang, B., Fang, H., Chen, B., Yang, S., Ye, Z., Yu, J., 2021. Effects of reductive inorganics and NOM on the formation of chlorite in the chlorine dioxide disinfection of drinking water. J. Environ. Sci. 104, 225–232. doi:10.1016/j.jes.2020.11.033.
Yang, X., Guo, W., Lee, W., 2013a. Formation of disinfection byproducts upon chlorine dioxide preoxidation followed by chlorination or chloramination of natural organic matter. Chemosphere 91, 1477–1485. doi:10.1016/j.chemosphere.2012.12.014.
Yang, X., Guo, W., Zhang, X., Chen, F., Ye, T., Liu, W., 2013b. Formation of disinfection by-products after pre-oxidation with chlorine dioxide or ferrate. Water Res 47, 5856–5864. doi:10.1016/j.watres.2013.07.010.
Yin, R., Shang, C., 2020. Removal of micropollutants in drinking water using UV-LED/chlorine advanced oxidation process followed by activated carbon adsorption. Water Res 185, 116297. doi:10.1016/j.watres.2020.116297.
Yin, R., Shen, P., Lu, Z., 2019. A green approach for the reduction of graphene oxide by the ultraviolet/sulfite process. J. Colloid Interface Sci. 550, 110–116. doi:10.1016/j.jcis.2019.04.073.
Zeng, T., Plewa, M.J., Mitch, W.A., 2016. N-Nitrosamines and halogenated disinfection byproducts in U.S. Full Advanced Treatment trains for potable reuse. Water Res 101, 176–186. doi:10.1016/j.watres.2016.03.062.
Zeng, Z., Wang, Y., Zhou, Q., Yang, K., Lin, D., 2019. New insight into the aggregation of graphene oxide in synthetic surface water: carbonate nanoparticle formation on graphene oxide. Environ. Pollut. 250, 366–374. doi:10.1016/j.envpol.2019.03.112.
Zhao, J., Shang, C., Zhang, X., Yang, X., Yin, R., 2021. The multiple roles of chlorite on the concentrations of radicals and ozone and formation of chlorate during UV photolysis of free chlorine. Water Res doi:10.1016/j.watres.2020.116680.